

# MRI-based Multi-task Decoupling Learning for Alzheimer’s Disease Detection and MMSE Score Prediction: A Multi-site Validation

Xu Tian, Jin Liu, Hulin Kuang, Yu Sheng, Jianxin Wang,  
and The Alzheimer’s Disease Neuroimaging Initiative <sup>\*†‡</sup>

## Abstract

Accurately detecting Alzheimer’s disease (AD) and predicting mini-mental state examination (MMSE) score are important tasks in elderly health by magnetic resonance imaging (MRI). Most of the previous methods on these two tasks are based on single-task learning and rarely consider the correlation between them. Since the MMSE score, which is an important basis for AD diagnosis, can also reflect the progress of cognitive impairment, some studies have begun to apply multi-task learning methods to these two tasks. However, how to exploit feature correlation remains a challenging problem for these methods. To comprehensively address this challenge, we propose a MRI-based multi-task decoupled learning method for AD detection and MMSE score prediction. First, a multi-task learning network is proposed to implement AD detection and MMSE score prediction, which exploits feature correlation by adding three multi-task interaction layers between the backbones of the two tasks. Each multi-task interaction layer contains two feature decoupling modules and one feature interaction module. Furthermore, to enhance the generalization between tasks of the features selected by the feature decoupling module, we propose the feature consistency

loss constrained feature decoupling module. Finally, in order to exploit the specific distribution information of MMSE score in different groups, a distribution loss is proposed to further enhance the model performance. We evaluate our proposed method on multi-site datasets. Experimental results show that our proposed multi-task decoupled representation learning method achieves good performance, outperforming single-task learning and other existing state-of-the-art methods.

**Keywords:** Alzheimer’s disease detection; MMSE score prediction; Multi-task decoupling learning; MRI;

## 1 Introduction

Alzheimer’s (AD) [1] is a common neurodegenerative disease common in the elderly. AD patients often suffer from memory, cognitive and motor impairments as the disease progresses [2]. As an important basis for AD detection, the Mini Mental State Examination (MMSE) [3] is often used clinically to assess the progress of elders’ cognitive and behavioral status. This assessment process is conducted in a question-and-answer format and is therefore often influenced by the patient’s subjective psychological state. AD not only affects the normal life of patients, but also greatly increases the cost of caring for the elderly for families and society. Therefore, accurate AD detection and MMSE score prediction are urgent for elder health.

Magnetic resonance imaging (MRI) is considered the most promising candidate due to its non-invasiveness and sensitivity to changes in brain struc-

<sup>\*</sup>This work is supported in part by the National Natural Science Foundation of China under Grant (No.62172444, No.62102454, and No.61877059), the 111 Project (No.B18059), and the Hunan Provincial Science and Technology Innovation Leading Plan (No.2020GK2019).

<sup>†</sup>Xu Tian, Jin Liu, Hulin Kuang, Yu Sheng and Jianxin Wang are with the Hunan Provincial Key Lab on Bioinformatics, School of Computer Science and Engineering, Central South University, Changsha, 410083, China

<sup>‡</sup>Corresponding author: Jin Liu.

ture. Specifically, hippocampal atrophy is considered a symptom strongly associated with cognitive impairment, making it an important basis for AD diagnosis and MMSE score prediction [4]. In the past few years, MRI has been widely used to distinguish AD patients from normal control (NC) subjects. In addition, since MMSE score is associated with AD, MRI has also been used to predict MMSE score. Some studies have shown that some handcrafted features obtained from MRI are significantly associated with symptoms such as cognitive impairment and behavioral disorders in the brain [5]-[6]. These methods often rely on multi-step pipelines [7]-[8]. To avoid suboptimal performance caused by handcrafted features, more and more deep learning-based methods have shown the potential to detect AD and predict MMSE score. Therefore, AD detection and MMSE score prediction are important issues in the field of MRI-based brain imaging.

Routine MRI images often reveal the progression of cognitive impairment through structural changes in specific brain regions. However, even clinicians have difficulty judging a patient’s dementia progression from MRI images due to the subtlety of brain structural changes. Furthermore, most of the existing fully automatic methods are based on single-task methods and do not consider the correlation between the two tasks. Therefore, jointly training these two tasks in the same deep learning network, encouraging feature sharing for AD detection and MMSE score prediction, and further improving the robustness of features is a promising research direction.

In this study, we propose a MRI-based multi-task decoupling learning (MTRL) method for AD detection and MMSE score prediction. The framework of our proposed method is shown in Fig. 1. First, we propose the same 3D CNN for AD detection and MMSE score prediction and add multi-task interaction layers composed of feature decoupling modules and feature interaction module between the backbone of the two tasks. The feature decoupling module is used to obtain the generalizable features of the two tasks, and the feature interaction module uses the correlation between the tasks by extracting the shared features. Then, a feature consistency loss is proposed to further constrain generalizable features,

which avoids constraining feature decoupling only by learning-based approaches. Finally, we specifically design the distribution loss related to the data distribution for MMSE score prediction. We use the subjects from phase 1 and 2 of the Alzheimer’s Disease Neuroimaging Initiative (ADNI1 and ADNI2: <http://adni.loni.usc.edu/>) and the Minimal Interval Resonance Imaging in Alzheimer’s Disease (MIRIAD: <http://miriad.drc.ion.ucl.ac.uk/>) to evaluate the method. Our main contributions are summarized as follows:

- 1) We develop an end-to-end multi-task learning network for AD detection and MMSE score prediction via multi-task interaction layers including feature decoupling modules and feature interaction module.
- 2) To further improve the effectiveness of multi-task interaction, a feature consistency loss is proposed to enhance the generalization of the features acquired by the feature decoupling modules.
- 3) In order to exploit the distribution information of MMSE scores in different groups, a distribution loss is constructed to improve the performance of MMSE score prediction.
- 4) To verify the robustness of our proposed method, we perform validation on multi-site datasets including ADNI1, ADNI2 and MIRIAD.

## 2 Related work

### 2.1 AD detection

MRI-based AD detection has always been a challenging problem. Early research on AD relied mainly on hand-crafted features [9]-[10]. These studies observed structural changes in the brain by measuring the volume of brain regions such as the hippocampus. However, handcrafted features sometimes fail to accurately identify small changes in brain structure. To further explore the subtle morphological changes in the brains of AD patients, many studies have used

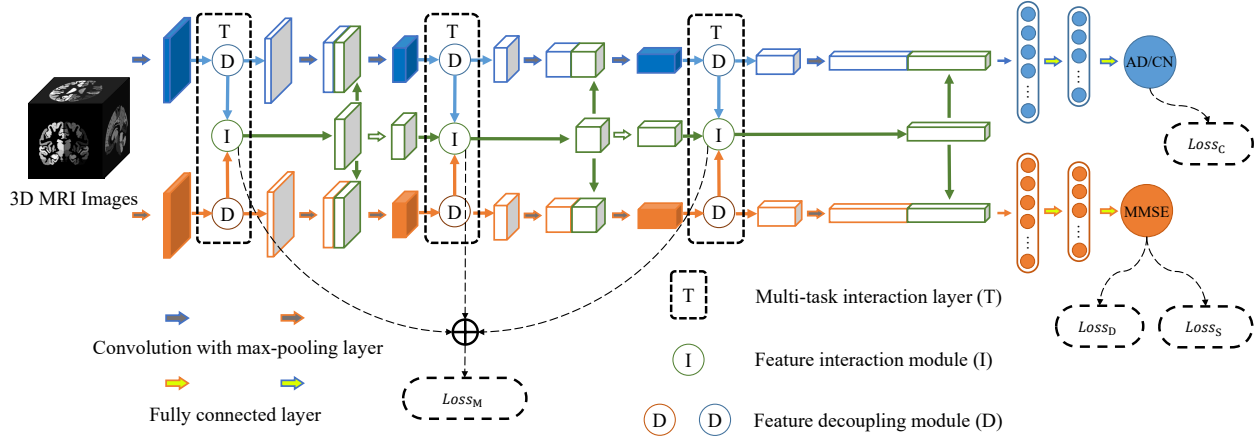


Figure 1: Framework of our proposed method

CNNs as the main framework for AD detection [11]-[12].

Depending on the input, CNN methods for AD detection can be classified into three categories: 2D slice-based, 3D region-of-interest (ROI)-based and 3D subject-based. AD detection methods based on 2D slices can learn from some classic methods in the field of computer vision, such as ResNet [13] and VGGNet [14]. To exploit the spatial information, some researchers selected some patches from 3D MRI images as the input of 3D CNN model [15]. Zhang et al. [16] proposed a landmark-based feature extraction method. The method first identified brain regions with significant differences between AD and CN and used these regions for AD detection. Like some selection methods based on prior knowledge [17], these methods ignore structural information in other brain regions. The 3D subject-level approach uses the subject's whole brain image as the input to the CNN. Some studies extend classical networks to 3D to accommodate 3D input [18]. Many researchers have also proposed new network structures. Qiu et al. [19] proposed an AD detection method consisting of a fully convolutional network (FCN) and a separate classification model. This method uses FCN to identify voxels that are more efficient for AD detection. As the etiology and associated brain regions of AD are not well understood, a 3D subject-based approach

is our choice.

## 2.2 MMSE score prediction

MMSE score are used clinically to measure cognitive status. But it is easily affected by the subjective status of the patient. To be able to objectively predict MMSE score, Kovacevic et al. [20] investigated the relationship between the volume of brain regions such as the hippocampus and the MMSE score. They sought to see if the volume of these brain regions could be used to predict changes in patients' MMSE score over the next 6 months. This study validated the feasibility of MRI as an objective criterion for predicting MMSE.

To more accurately predict MMSE score, Huang et al. [21] proposed a random forest (RF) method based on nonlinear sparse regression to predict MMSE score. This method combined the prediction results of different paths in RF by probability. Further, Tabarestani et al. [22] proposed a CNN-based MMSE score prediction method. The method also treats clinical scoring at different time points as multiple tasks and develops a multi-task regression model. Furthermore, Liu et al. [23] used weakly supervised deep learning to predict clinical information including MMSE score. They constructed a new loss to exploit incompletely labeled data. The increase in available

data enhanced the robustness of the model. It can be seen that the CNN-based method has become the mainstream method for MMSE score prediction.

### 2.3 Joint detection and prediction

MMSE score is one of the basis for clinical diagnosis of AD. Due to the correlation between MMSE scores and AD, Duc et al. [24] proposed AD detection and MMSE score prediction methods. They developed a 3D CNN-based AD detection method and applied multiple regression methods including linear least squares regression to MMSE score prediction. Although this method completes AD detection and MMSE score prediction, it did not perform multi-task joint learning. So it could not improve model performance through relationships between tasks.

Zhu et al. [25] proposed a multi-task approach for AD detection and MMSE score prediction. The method combined multi-task feature selection with a new matrix similarity-based loss function. Different from hand-crafted feature-based methods, Liu et al. [26] proposed a 3D patch-based method for these tasks. The method identified brain regions with significant differences between AD and NC, and then extracted multiple patches around these landmarks for AD detection and MMSE score prediction. To take advantage of richer patient information, EI Sappagh et al. [27] added MRI data and genetic data as input to a multi-task approach to complete AD detection and MMSE score prediction. They perform multi-modal feature fusion via BiLSTM and finally implement multiple tasks on different fully connected layers. Through the above studies, we consider that the use of multi-task learning for AD detection and MMSE score prediction has become an active topic.

## 3 Method

### 3.1 Multi-task learning network

Fig. 1 shows the proposed 3D multi-task learning network, which include backbones to perform AD detection and MMSE score prediction and three multi-task interaction layers (T). Specifically, the multi-

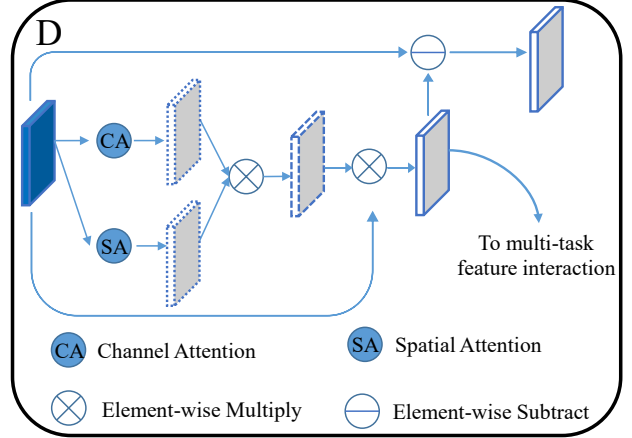


Figure 2: Feature decoupling module (D)

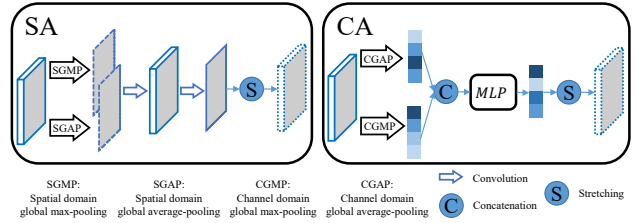


Figure 3: Spatial attention module (SA) and Channel attention module (CA)

task interaction layer include two feature decoupling modules (D) and a feature interaction module (I). It obtain generalizable features from the features in the backbones through feature decoupling module, and interacts to obtain shared features through feature interaction module. This network is denoted as MTDL.

#### 3.1.1 Multi-task interaction layer

There are correlations and specificities between the features of different tasks, which makes the features of one task not always effective for another task. Therefore, the feature decoupling module is proposed to select generalizable features and avoid feature redundancy before the feature interaction module.

As is shown in Fig. 2, the channel attention (CA)

[28] and spatial attention (SA) [29] is used to generate new feature-level attention. As is shown in Fig. 3, global average pooling (GAP) and global max pooling (GMP) are used to obtain information in channel and spatial domain. Then, a multi-layer perceptron (MLP) and convolution layers are used respectively to get the attention map in channel and spatial domain. They can be defined as follow:

$$\begin{aligned} \text{CA}(\mathbf{Z}^l) &= \text{S}(\text{MLP}(\text{Concat}(\text{CGAP}(\mathbf{Z}^l), \text{CGMP}(\mathbf{Z}^l)))), \\ \text{SA}(\mathbf{Z}^l) &= \text{S}(\text{E}_{\text{SA}}(\text{Concat}(\text{SGAP}(\mathbf{Z}^l), \text{SGMP}(\mathbf{Z}^l)))), \end{aligned} \quad (1)$$

where  $\mathbf{Z}^l$  is the feature map output of  $l$ th layer of CNN, CGAP and CGMP denote global average pooling and global max pooling in channel domain, SGAP and SGMP denote global average pooling and global max pooling in spatial domain, Concat denotes the concatenation of features, MLP denotes a multi-layer perceptron,  $\text{E}_{\text{SA}}$  denotes encoding layer containing two convolution layers, and S denotes stretching the attention map to the original input size.

The feature decoupling module multiplies the channel domain and spatial domain attention maps element-wise to get the weight of each feature. Then, it is used to select generalizable features. The rest of the features will remain in the backbone. Feature decoupling modules can be defined as follow:

$$\mathbf{Z}_G^l = (\text{CA}(\mathbf{Z}_O^l) \cdot \text{SA}(\mathbf{Z}_O^l)) \cdot \mathbf{Z}_O^l, \quad (3)$$

$$\mathbf{Z}_{N-G}^l = \mathbf{Z}_O^l - \mathbf{Z}_G^l, \quad (4)$$

where  $\mathbf{Z}_O^l$  is the original features from the  $l$ th layer of backbone,  $\mathbf{Z}_G^l$  is the generalizable features filtered by the feature decoupling module, and  $\mathbf{Z}_{N-G}^l$  is the non-generalizable features.

Two feature decoupling modules are used to obtain generalizable features from the backbone of AD detection and MMSE score prediction respectively. Then, as is shown in Fig. 4, these generalizable features continue to be used for feature interaction to obtain shared features.

Feature interaction can be done by linear transformation of different task features. Misra et al. [30] proposed linear transformation of feature maps by learnable weights. This method forces different brain

regions to share weights when participating in linear transformations. However, both AD detection and MMSE score prediction have their more focused brain regions. Furthermore, we consider that the correlation between AD detection and MMSE score prediction was not the same for different subjects. Therefore, the attention module is used to obtain the weights of the linear transformation, which is the same as the attention module used for feature decoupling. The attention mechanism makes the same feature have different weights to linear transformation for different subjects. In addition, convolution can not only provide useful information for feature interaction, but also correct possible feature misalignment, that is, the spatial correspondence between the feature and the original image is not completely accurate. Therefore, convolutions are used to obtain the residual and correct the shared features obtained based on linear transformation, after changing its number of channels using  $1 \times 1 \times 1$  convolution.

Features at different scales have different semantic information. For feature interaction at multiple scales, the feature interaction module returns the shared feature to the backbone network of the task, concatenating it with the retained non-generalizable features to influence subsequent feature extraction. Meanwhile, convolution and pooling are used to make non-generalizable features have the same dimension as shared features.

Shared features are consistent, that is, the shared features extracted by the previous interaction module can provide useful information for subsequent feature interactions. Therefore, after necessary convolution and pooling, we feed the shared features obtained by the first feature interaction module to the second module. To sum up, the feature interaction module can be defined as follows:

$$\begin{aligned} \mathbf{Z}_L^l &= (\text{CA}(\mathbf{Z}_{A,G}^l) \cdot \text{SA}(\mathbf{Z}_{A,G}^l)) \cdot \mathbf{Z}_{A,G}^l \\ &\quad + (\text{CA}(\mathbf{Z}_{M,G}^l) \cdot \text{SA}(\mathbf{Z}_{M,G}^l)) \cdot \mathbf{Z}_{M,G}^l, \end{aligned} \quad (5)$$

$$\mathbf{Z}_R^l = \text{E}_I(\text{Concat}(\mathbf{Z}_{A,G}^l, \mathbf{Z}_{M,G}^l, \text{E}_S(\mathbf{Z}_S^{l-1}))), \quad (6)$$

$$\mathbf{Z}_S^l = \text{ReLU}(\text{Conv}_{1 \times 1 \times 1}(\mathbf{Z}_L^l)) + \mathbf{Z}_R^l, \quad (7)$$

where  $\mathbf{Z}_{A,G}^l$  and  $\mathbf{Z}_{M,G}^l$  is the generalizable features extracted from the backbone of AD detection and

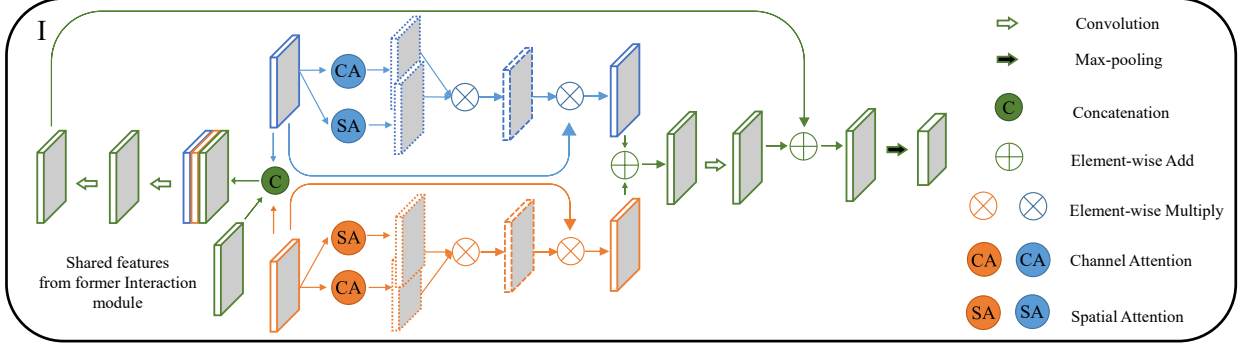


Figure 4: Feature Interaction module (I)

MMSE prediction in layer  $l$ ,  $\mathbf{Z}_L^l$  is the shared features obtained by linear transformation,  $\mathbf{Z}_R^l$  is the residuals used to correct the  $\mathbf{Z}_L^l$ ,  $\mathbf{Z}_S^l$  is the shared features extracted from the generalizable features,  $E_I$  contains two convolutional layers, and  $E_S$  contains a convolution and a max pooling.

### 3.1.2 AD detection

After the feature extraction stage, two fully connected layers are used to perform the AD detection task. In the AD detection task, we use the cross-entropy loss:

$$\mathcal{L}_C = \frac{1}{N} \sum_{i=1}^N -(y_i \log(p_i) + (1 - y_i) \log(1 - p_i)) , \quad (8)$$

where  $y_i$  denotes the label of  $i$ th subject, and  $p_i$  denotes the probability that the  $i$ th subject is a AD patient.

### 3.1.3 MMSE score prediction

Similar to AD detection, two fully connected layers are used to predict subjects' MMSE scores. For the MMSE score prediction task, we use the smooth L1 loss:

$$\mathcal{L}_S = \begin{cases} 0.5(m_i - \hat{m}_i)^2 & |m_i - \hat{m}_i| < 1 \\ |m_i - \hat{m}_i| - 0.5 & \text{otherwise} \end{cases} , \quad (9)$$

$$\mathcal{L}_S = \frac{1}{N} \sum_{i=1}^N \mathcal{L}_s , \quad (10)$$

where  $m_i$  denotes the true value of MMSE score of  $i$ th subject, and  $\hat{m}_i$  denotes the predicted value of MMSE score of  $i$ th subject.

To implement multi-task joint learning, the joint loss is defined as follows:

$$\mathcal{L}_J = \alpha_C \mathcal{L}_C + \alpha_S \mathcal{L}_S , \quad (11)$$

where  $\alpha_C$  and  $\alpha_S$  denote the weights of  $\mathcal{L}_C$  and  $\mathcal{L}_S$  respectively.

## 3.2 The feature consistency loss

In multi-task interaction layer, the generalizable features are extracted in a learning-based manner. However, it is sometimes unreliable to rely on only learning-based feature decoupling. We consider that generalizable features usually have a consistent distribution. Therefore, the feature consistency loss  $\mathcal{L}_{fc}$  is proposed to measure the difference between the distributions of generalizable features, which performs average pooling and maximum pooling of the generalizable features of AD detection and MMSE score prediction in the spatial domain, and uses the perceptual loss to measure their difference.  $\mathcal{L}_{fc}$  can be defined as follows:

$$\mathcal{L}_{fc} = \|\text{SGMP}(\mathbf{Z}_{A,G}^l) - \text{SGMP}(\mathbf{Z}_{M,G}^l)\|_1 + \|\text{SGAP}(\mathbf{Z}_{A,G}^l) - \text{SGAP}(\mathbf{Z}_{M,G}^l)\|_1 , \quad (12)$$

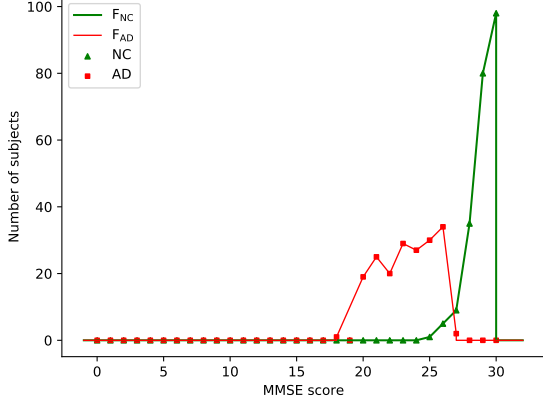


Figure 5: MMSE score distribution with different groups in ADNI1 dataset and function  $F_c(x)$

where  $\mathbf{Z}_{A,G}^l$  and  $\mathbf{Z}_{M,G}^l$  are the generalizable features obtained from the AD detection task and the MMSE score prediction task, respectively, SGMP and SGAP respectively represent the max pooling and average pooling in spatial domain.

In MTDL, we use the loss  $\mathcal{L}_M$  to constrain the generalizable features for three multi-task interaction layers, and realize the deep supervision of feature decoupling. As is shown in Fig. 1, it can be defined as follows:

$$\mathcal{L}_M = \frac{1}{N} \sum_{i=1}^N \sum_{l=1}^L \mathcal{L}_{fc}, \quad (13)$$

where  $N$  is the number of subjects,  $L = 3$  is the number of layers involved in the feature interaction.

### 3.3 The distribution loss of MMSE score prediction task

MMSE score prediction differs from AD detection in that it has multiple truth values to fit on a single output neuron. From the perspective of the whole dataset, the MMSE scores have a certain distribution pattern on the AD group and the NC group. The distribution of MMSE score on the ADNI1 dataset is shown in Fig. 5. However, the loss  $\mathcal{L}_S$  for MMSE

score prediction does not exploit information from this perspective. Therefore, the output of the network should be fitted at the distribution level in addition to being fitted at the subject level.

The original data distribution is not suitable for calculation, because it only contains discrete points and the domain of definition is finite. Therefore, an improved data distribution function is used to replace it. We only select discrete points whose function value is not 0 from the distribution to construct a function  $F_c(x)$  by connecting them using linear functions.  $A_c$  is the domain of definition corresponding to these selected discrete points. Then, the distribution loss with the distribution function  $F_c(x)$  can be defined as follows:

$$\mathcal{L}_d = \frac{(\int_{m_i}^{\hat{m}_i} F_c(x) dx)^2}{AU(F_c)}, c \in \{AD, NC\}, \quad (14)$$

$$\frac{\partial \mathcal{L}_d}{\partial \hat{m}_i} = \frac{2 \int_{m_i}^{\hat{m}_i} F_c(x) dx \cdot F_c(\hat{m}_i)}{AU(F_c)}, c \in \{AD, NC\}, \quad (15)$$

$$\mathcal{L}_D = \frac{1}{N} \sum_{i=1}^N \mathcal{L}_d, \quad (16)$$

where  $m_i$  denotes the true value of MMSE score of  $i$ th subject,  $\hat{m}_i$  denotes the predicted value of MMSE score of  $i$ th subject, and  $AU(f)$  is the area under the function  $f$  and is used to normalize the definite integral of the function  $f$ .

During model training, we find that  $\mathcal{L}_d$  has a gradient  $\nabla \mathcal{L}_d$  of 0 sometime, which makes it impossible to backpropagate. Therefore, as shown in **Algorithm 1**, we modify  $\nabla \mathcal{L}_d$  to a fixed value according to certain rules to ensure stable training when it is 0.

In summary, the total loss of our proposed MTDL can be defined as follows:

$$\mathcal{L}_{total} = \mathcal{L}_J + \alpha_M \mathcal{L}_M + \alpha_D \mathcal{L}_D, \quad (17)$$

$$\mathcal{L}_J = \alpha_C \mathcal{L}_C + \alpha_S \mathcal{L}_S, \quad (18)$$

where  $\alpha_C$ ,  $\alpha_S$ ,  $\alpha_M$ ,  $\alpha_D$  denote the weights of  $\mathcal{L}_C$ ,  $\mathcal{L}_S$ ,  $\mathcal{L}_M$  and  $\mathcal{L}_D$  respectively.

---

**Algorithm 1** Solve  $\nabla \mathcal{L}_d$  for  $i$ th subject

---

**Input:**  $F_{AD}(x)$ ,  $F_{CN}(x)$ ,  $A_{AD}$ ,  $A_{CN}$ ,  $y_i$ ,  $m_i$ ,  $\hat{m}_i$ , the parameters of MTDL in  $t$  epoch  $\theta_t$  and the scaling factor  $\lambda$

```
1:  $c \leftarrow y^i$ 
2: if  $\min(A_c) \leq \hat{m}^i \leq \max(A_c)$  then
3:    $\nabla \mathcal{L}'_d \leftarrow \frac{\partial \mathcal{L}_d}{\partial \hat{m}_i}$ 
4: else
5:   if  $\hat{m}^i < \min(A_c)$  then
6:      $\nabla \mathcal{L}'_d \leftarrow -\lambda F_c(\min(A_c))$ 
7:   else
8:      $\nabla \mathcal{L}'_d \leftarrow \lambda F_c(\max(A_c))$ 
9:   end if
10: end if
11:  $\nabla \mathcal{L}'_d \leftarrow \nabla \mathcal{L}'_d \frac{\partial \hat{m}_i}{\partial \theta_t}$ 
```

**Output:**  $\nabla \mathcal{L}'_d$

---

### 3.4 Explainable analysis

To further validate our proposed method, the interpretability analysis should be used to verify the correlation between these two tasks. The correlation of the two tasks means that the two tasks have the same or partially the same ROIs.

We back-propagates the output of the network to the original input space. The larger the absolute value of the gradient in a certain region, it means that the network has a higher sensitivity to the region. The sensitivity map  $s$  can be calculated as follows:

$$S_{[i,j,k]} = \left| \frac{\partial y}{\partial X_{[i,j,k]}} \right|, \quad (19)$$

where  $s$  is the sensitivity map,  $x$  is the original input image, and  $y$  is the output of the network, which may be the probability of AD detection or the predicted value of MMSE score. In addition, the gradient-based method faces the problem of noise. This makes the gradient of the model appear irregular fluctuations. In order to solve this issue, we perform down-sampling and up-sampling of the sensitivity map to optimize its display after normalization.

## 4 Experiments and Results

### 4.1 Data

In this study, we select subjects from the ADNI dataset and the MIRIAD dataset to evaluate our proposed MTDL. The data we used include 187 AD patients and 228 NC subjects selected from the ADNI1 dataset and 84 AD patients and 137 NC subjects selected from the ADNI2 dataset. The MIRIAD dataset is a volumetric MRI brain scan database of 46 AD patients and 23 NC subjects. The study aims to investigate the feasibility of using MRI as a measure of the outcome of clinical trials for the treatment of AD. Table 1 summarizes the detailed information of the subjects we selected.

The FSL [31] software package is used to preprocess the MRI images. First of all, the FIRST tool is used to register all the original MRI images into the MNI152 standard template. Subsequently, the BET tool is used to remove the skull from the MRI images. Then, in order to further improve the image quality, we use z-score normalization to normalize the intensity of the voxels in the images and removed the background.

### 4.2 Experimental settings

The ADNI1 dataset is randomly divided into 10 equal parts. They take turns as the test set and validation set in 10 experiments. The ADNI2 dataset and the MIRIAD dataset are external validation set. In each experiment, we only use the training set to construct  $F_{NC}(x)$  and  $F_{AD}(x)$ . Definite integrals are calculated using the trapezoidal rule. The loss weights  $\alpha_C$ ,  $\alpha_S$ ,  $\alpha_M$  and  $\alpha_D$  are set as 1, 1, 1 and 0.5, respectively. The parameter  $\lambda$  in **Algorithm 1** is set to 0.5. We choose the model that performs best on the validation set for testing. It is worth mentioning that, the performance of the AD detection task is first concern when choosing the optimal model. The parameter optimization algorithm we used is the Adam method [32]. The number of epochs in each experiment is 300. The learning rate is  $10^{-4}$ . The batch size is 2. All experiments is performed on NVIDIA GTX2080.

For AD detection task, we use four metrics to eval-

Table 1: Demographic information of the subjects involved in this study (mean  $\pm$  std)

Dataset	Group	Sex (male/female)	Age (year)	MMSE
ADNI1	AD	101/86	75.43 $\pm$ 7.50	23.35 $\pm$ 2.05
	NC	119/109	76.00 $\pm$ 5.01	29.11 $\pm$ 1.00
ADNI2	AD	55/29	75.74 $\pm$ 8.37	21.90 $\pm$ 3.10
	NC	73/64	74.88 $\pm$ 6.13	28.93 $\pm$ 1.21
MIRIAD	AD	19/27	69.34 $\pm$ 6.98	19.20 $\pm$ 3.97
	NC	12/11	69.66 $\pm$ 7.02	29.39 $\pm$ 0.82

uate the performance of the model, including accuracy (ACC), sensitivity (SEN), specificity (SPE) and area under the receiver operating characteristic curve (AUC) value. These metrics are defined as:

$$\text{ACC} = \frac{\text{TP} + \text{TN}}{\text{TP} + \text{TN} + \text{FP} + \text{FN}} , \quad (20)$$

$$\text{SEN} = \frac{\text{TP}}{\text{TP} + \text{FN}} , \quad (21)$$

$$\text{SPE} = \frac{\text{TN}}{\text{TN} + \text{FP}} , \quad (22)$$

where TP, TN, FP and FN denote true positive, true negative, false positive and false negative respectively. For the MMSE score prediction task, we use root mean square error (RMSE) and the Pearson correlation coefficient ( $r$ ) as the metrics. They are defined as:

$$\text{RMSE} = \sqrt{\frac{1}{N} \sum_{i=1}^N (m_i - \hat{m}_i)^2} , \quad (23)$$

$$r = \frac{\sum_{i=1}^N (m_i - \bar{m})(\hat{m}_i - \bar{\hat{m}})}{\sqrt{\sum_{i=1}^N (m_i - \bar{m})^2} \sqrt{\sum_{i=1}^N (\hat{m}_i - \bar{\hat{m}})^2}} , \quad (24)$$

where  $N$  denotes the number of subjects, and  $m_i$  denotes the true value of MMSE score of  $i$ th subject, and  $\hat{m}_i$  denotes the predicted value of MMSE score of  $i$ th subject, and  $\bar{m}$  denotes the mean value of all true MMSE score, and  $\bar{\hat{m}}$  denotes the mean value of all predicted values of MMSE score.

### 4.3 Ablation experiment

Our proposed MTDL contains multiple effective modules. In this subsection, we verify the effectiveness of these components.

#### 4.3.1 Multi-task interaction layer

In MTDL, we propose the multi-task interaction layer. To verify the effectiveness, we remove it from MTDL. The network becomes single-task learning networks for AD detection and MMSE score prediction. We name the networks for AD detection and MMSE score prediction as ST-Net<sub>A</sub> and ST-Net<sub>M</sub>, respectively. In addition, the consistency of shared functions enables subsequent functional interaction modules to acquire information from previous functional interaction modules. To test this hypothesis, we removed the connection between the interaction modules in MTDL and named it MTDL<sub>NonC</sub>. The performance comparison between these models and MTDL is shown in Table 2. In the ADNI1 dataset, our proposed MTDL achieves an ACC of 87.26%, a SEN of 84.41%, a SPE of 89.78% and an AUC of 95.45% for AD detection, achieves a RMSE of 2.50 and a  $r$  of 0.73. In the ADNI2 dataset, our proposed MTDL achieves an ACC of 86.33%, a SEN of 78.43%, a SPE of 91.00% and an AUC of 93.35% for AD detection, achieves a RMSE of 2.92 and a  $r$  of 0.76. In the MIRIAD dataset, our proposed MTDL achieves an ACC of 93.63%, a SEN of 94.13%, a SPE of 93.23% and an AUC of 99.16% for AD detection, achieves a RMSE of 4.78 and a  $r$  of 0.72. The multi-task interaction layers effectively enhances the robustness of the representation. The connections between multi-task interaction layers enhance the stability of shared representations.

#### 4.3.2 Multi-layer feature consistency loss of MTDL

In MTDL, we adopt a multi-layer feature consistency loss to further constrain the feature decoupling module. It enhances the consistency of generalizable fea-

Table 2: Comparison of AD detection and MMSE score prediction performance of ST-Net<sub>A</sub>, ST-Net<sub>M</sub>, MTDL<sub>NonC</sub> and MTDL (mean  $\pm$  std)

Datasets	Methods	AD detection				MMSE score prediction	
		ACC (%)	SEN (%)	SPE (%)	AUC (%)	RMSE	r
ADNI1	ST-Net <sub>A</sub>	77.65 $\pm$ 3.54	71.34 $\pm$ 6.80	84.89 $\pm$ 5.23	88.35 $\pm$ 2.99	-	-
	ST-Net <sub>M</sub>	-	-	-	-	3.57 $\pm$ 0.78	0.42 $\pm$ 0.09
	MTDL <sub>NonC</sub>	84.46 $\pm$ 6.97	79.20 $\pm$ 12.14	87.15 $\pm$ 9.20	91.27 $\pm$ 3.92	2.50 $\pm$ 0.22	0.69 $\pm$ 0.07
	MTDL	<b>87.26 <math>\pm</math> 4.32</b>	<b>84.41 <math>\pm</math> 5.51</b>	<b>89.78 <math>\pm</math> 5.61</b>	<b>94.45 <math>\pm</math> 4.02</b>	<b>2.50 <math>\pm</math> 0.15</b>	<b>0.73 <math>\pm</math> 0.06</b>
ADNI2	ST-Net <sub>A</sub>	75.34 $\pm$ 3.95	68.57 $\pm$ 12.00	<b>92.54 <math>\pm</math> 7.52</b>	87.74 $\pm$ 2.27	-	-
	ST-Net <sub>M</sub>	-	-	-	-	3.93 $\pm$ 0.43	0.30 $\pm$ 0.06
	MTDL <sub>NonC</sub>	84.34 $\pm$ 2.52	<b>83.59 <math>\pm</math> 8.98</b>	84.83 $\pm$ 8.51	92.73 $\pm$ 1.27	3.06 $\pm$ 0.21	0.74 $\pm$ 0.04
	MTDL	<b>86.33 <math>\pm</math> 2.37</b>	78.43 $\pm$ 6.74	91.00 $\pm$ 3.89	<b>93.35 <math>\pm</math> 1.53</b>	<b>2.92 <math>\pm</math> 0.16</b>	<b>0.76 <math>\pm</math> 0.02</b>
MIRIAD	ST-Net <sub>A</sub>	81.35 $\pm$ 4.34	70.69 $\pm$ 13.23	<b>92.56 <math>\pm</math> 3.67</b>	87.64 $\pm$ 0.07	-	-
	ST-Net <sub>M</sub>	-	-	-	-	5.08 $\pm$ 0.24	0.30 $\pm$ 0.03
	MTDL <sub>NonC</sub>	92.46 $\pm$ 4.52	<b>95.16 <math>\pm</math> 3.93</b>	86.95 $\pm$ 11.95	98.58 $\pm$ 0.01	4.85 $\pm$ 0.39	0.69 $\pm$ 0.05
	MTDL	<b>93.63 <math>\pm</math> 2.21</b>	94.13 $\pm$ 2.58	93.23 $\pm$ 4.58	<b>99.16 <math>\pm</math> 1.14</b>	<b>4.78 <math>\pm</math> 0.24</b>	<b>0.72 <math>\pm</math> 0.03</b>

tures from different tasks by constraining the feature distribution of AD detection and MMSE score prediction. To verify the effectiveness of this loss, we add  $\mathcal{L}_M$  to MTDL with only  $\mathcal{L}_C$  and  $\mathcal{L}_S$ . In addition, we also remove  $\mathcal{L}_M$  from MTDL. As shown in Table 3, for the AD detection task, the loss  $\mathcal{L}_M$  improves the ACC, SPE and AUC of the base network by 2.09%, 1.56% and 0.64% respectively in the ADNI1 dataset. For the MMSE score prediction task, it reduces the RMSE by 0.11.  $\mathcal{L}_M$  further enhances the effectiveness of multi-task feature decoupling by constraining generalizable features from different tasks.

#### 4.3.3 Distribution loss of MTDL

In MTDL, we also propose a distribution loss  $\mathcal{L}_D$  for the MMSE score prediction task. It provides additional supervision for the MMSE score prediction task through the data distribution composed of all subjects in the dataset and makes the data distribution of MMSE score predictors closer to the true distribution. Similarly, to verify its effectiveness, we first add  $\mathcal{L}_D$  to MTDL with only  $\mathcal{L}_C$  and  $\mathcal{L}_S$ . We also remove  $\mathcal{L}_D$  from MTDL. As shown in Table 3, for the AD detection task, the loss  $\mathcal{L}_D$  improves the ACC, SPE and AUC of the base network by 1.29%, 4.44% and 1.81% respectively in the ADNI1 dataset. For the MMSE score prediction task, it reduces the RMSE by 0.37 and improves the r by 0.12. The distribution loss effectively reduces the error of the MMSE score prediction task and increases the correlation between the predicted and true values.

## 4.4 Comparison of MTDL with the state-of-the-art methods

To verify the superiority of our proposed MTDL, we compare it with a variety of existing multi-task feature interaction methods, including the hard sharing method [26], NDDR-CNN [33], cross-stitch [30], MTFIL-Net [34] and MTI-Net [35]. We replace the multi-task interaction layer in MTDL with the multi-task interaction module in these methods. We implement these feature interaction methods as described above. As shown in the table 4, we compare these interaction methods with MTDL in AD detection and MMSE score prediction. In the ADNI1 dataset, our proposed MTDL achieves an ACC of 87.26%, a SEN of 84.41%, a SPE of 89.78% and an AUC of 95.45% for AD detection, achieves a RMSE of 2.50 and a r of 0.73. Among all multi-task feature interaction methods, our method is the best on most performance metrics.

## 5 Discussion

### 5.1 Explainable analysis

AD patients often have memory impairment and cognitive impairment. These symptoms are often closely related to the hippocampus. Therefore, the ROI of AD detection task and MMSE score prediction task may be related to the hippocampus. We randomly select a total of 6 subjects from the test set and

Table 3: Comparison of AD detection and MMSE score prediction performance of MTDL with different loss (mean  $\pm$  std)

Datasets	Loss				AD detection				MMSE score prediction	
	$\mathcal{L}_C$	$\mathcal{L}_S$	$\mathcal{L}_D$	$\mathcal{L}_M$	ACC (%)	SEN (%)	SPE (%)	AUC (%)	RMSE	r
ADNI1	✓	✓			82.44 $\pm$ 6.88	81.25 $\pm$ 9.45	83.70 $\pm$ 7.85	90.53 $\pm$ 4.41	3.12 $\pm$ 0.32	0.61 $\pm$ 0.05
	✓		✓		83.73 $\pm$ 5.65	76.90 $\pm$ 7.68	88.14 $\pm$ 4.89	92.34 $\pm$ 6.27	2.75 $\pm$ 0.58	0.68 $\pm$ 0.07
	✓	✓		✓	84.53 $\pm$ 6.95	81.75 $\pm$ 7.56	85.26 $\pm$ 4.24	91.17 $\pm$ 3.11	3.01 $\pm$ 0.34	0.58 $\pm$ 0.05
	✓	✓	✓	✓	<b>87.26 <math>\pm</math> 4.32</b>	<b>84.41 <math>\pm</math> 5.51</b>	<b>89.78 <math>\pm</math> 5.61</b>	<b>94.45 <math>\pm</math> 4.02</b>	<b>2.50 <math>\pm</math> 0.15</b>	<b>0.73 <math>\pm</math> 0.06</b>
ADNI2	✓	✓			84.29 $\pm$ 5.11	<b>83.59 <math>\pm</math> 8.45</b>	85.11 $\pm$ 11.51	91.39 $\pm$ 1.16	3.89 $\pm$ 0.38	0.56 $\pm$ 0.04
	✓	✓	✓		84.86 $\pm$ 4.59	78.57 $\pm$ 8.26	88.54 $\pm$ 7.73	93.31 $\pm$ 3.09	3.25 $\pm$ 0.28	0.73 $\pm$ 0.03
	✓	✓		✓	84.61 $\pm$ 1.72	75.44 $\pm$ 10.61	90.05 $\pm$ 5.71	92.34 $\pm$ 1.62	3.84 $\pm$ 0.39	0.57 $\pm$ 0.08
	✓	✓	✓	✓	<b>86.33 <math>\pm</math> 2.37</b>	78.43 $\pm$ 6.74	<b>91.00 <math>\pm</math> 3.89</b>	<b>93.35 <math>\pm</math> 1.53</b>	<b>2.92 <math>\pm</math> 0.16</b>	<b>0.76 <math>\pm</math> 0.02</b>
MIRIAD	✓	✓			90.16 $\pm$ 3.69	93.91 $\pm$ 5.39	85.65 $\pm$ 11.93	98.31 $\pm$ 1.60	5.53 $\pm$ 0.61	0.59 $\pm$ 0.04
	✓	✓	✓		92.61 $\pm$ 2.28	93.96 $\pm$ 3.39	89.13 $\pm$ 9.17	98.54 $\pm$ 0.93	5.08 $\pm$ 0.37	0.68 $\pm$ 0.06
	✓	✓		✓	92.75 $\pm$ 2.55	94.02 $\pm$ 5.18	89.67 $\pm$ 11.49	98.13 $\pm$ 0.05	5.68 $\pm$ 0.26	0.61 $\pm$ 0.09
	✓	✓	✓	✓	<b>93.63 <math>\pm</math> 2.21</b>	<b>94.13 <math>\pm</math> 2.58</b>	<b>93.23 <math>\pm</math> 4.58</b>	<b>99.16 <math>\pm</math> 1.14</b>	<b>4.78 <math>\pm</math> 0.24</b>	<b>0.72 <math>\pm</math> 0.03</b>

Table 4: Comparison of AD detection and MMSE score prediction performance of the state-of-the-art methods and MTDL (mean  $\pm$  std)

Datasets	Methods	AD detection				MMSE score prediction	
		ACC (%)	SEN (%)	SPE (%)	AUC (%)	RMSE	r
ADNI1	hard sharing[26]	80.36 $\pm$ 8.89	82.63 $\pm$ 8.11	81.37 $\pm$ 11.74	90.20 $\pm$ 4.08	3.44 $\pm$ 0.37	0.59 $\pm$ 0.10
	cross-stitch[30]	83.01 $\pm$ 7.09	72.67 $\pm$ 17.24	93.58 $\pm$ 6.90	92.28 $\pm$ 4.83	2.91 $\pm$ 0.45	0.67 $\pm$ 0.09
	NDDR-CNN[33]	80.02 $\pm$ 4.70	80.11 $\pm$ 9.87	81.73 $\pm$ 10.68	89.98 $\pm$ 5.82	3.87 $\pm$ 0.89	0.57 $\pm$ 0.10
	MTFIL-Net[34]	82.18 $\pm$ 5.00	82.17 $\pm$ 8.15	84.35 $\pm$ 11.54	90.98 $\pm$ 3.99	2.90 $\pm$ 0.55	0.59 $\pm$ 0.10
	MTI-Net[35]	81.46 $\pm$ 5.47	74.23 $\pm$ 11.83	87.60 $\pm$ 6.71	89.52 $\pm$ 6.12	2.70 $\pm$ 0.27	0.63 $\pm$ 0.11
	MTDL	<b>87.26 <math>\pm</math> 4.32</b>	<b>84.41 <math>\pm</math> 5.51</b>	<b>89.78 <math>\pm</math> 5.61</b>	<b>94.45 <math>\pm</math> 4.02</b>	<b>2.50 <math>\pm</math> 0.15</b>	<b>0.73 <math>\pm</math> 0.06</b>
ADNI2	hard sharing[26]	79.68 $\pm$ 8.59	<b>88.75 <math>\pm</math> 6.15</b>	74.12 $\pm$ 11.93	90.70 $\pm$ 1.71	3.89 $\pm$ 0.29	0.61 $\pm$ 0.07
	cross-stitch[30]	82.26 $\pm$ 3.33	70.50 $\pm$ 13.76	90.70 $\pm$ 5.51	92.65 $\pm$ 2.19	3.32 $\pm$ 0.42	0.71 $\pm$ 0.07
	NDDR-CNN[33]	80.93 $\pm$ 5.18	71.16 $\pm$ 10.48	87.51 $\pm$ 14.01	90.41 $\pm$ 1.09	3.95 $\pm$ 0.60	0.59 $\pm$ 0.08
	MTFIL-Net[34]	84.47 $\pm$ 5.07	86.19 $\pm$ 5.35	83.43 $\pm$ 9.92	92.07 $\pm$ 1.97	3.43 $\pm$ 0.53	0.64 $\pm$ 0.04
	MTI-Net[35]	82.80 $\pm$ 4.35	70.83 $\pm$ 13.78	90.14 $\pm$ 6.89	91.65 $\pm$ 6.12	3.36 $\pm$ 0.19	0.67 $\pm$ 0.05
	MTDL	<b>86.33 <math>\pm</math> 2.37</b>	78.43 $\pm$ 6.74	<b>91.00 <math>\pm</math> 3.89</b>	<b>93.35 <math>\pm</math> 1.53</b>	<b>2.92 <math>\pm</math> 0.16</b>	<b>0.76 <math>\pm</math> 0.02</b>
MIRIAD	hard sharing[26]	90.30 $\pm$ 3.34	93.92 $\pm$ 6.24	84.05 $\pm$ 8.63	97.87 $\pm$ 6.27	5.56 $\pm$ 0.46	0.60 $\pm$ 0.09
	cross-stitch[30]	91.14 $\pm$ 2.59	91.54 $\pm$ 5.46	90.33 $\pm$ 11.73	98.61 $\pm$ 1.07	4.96 $\pm$ 0.32	0.69 $\pm$ 0.06
	NDDR-CNN[33]	89.60 $\pm$ 4.68	89.13 $\pm$ 7.31	84.54 $\pm$ 10.67	97.06 $\pm$ 1.46	5.34 $\pm$ 0.34	0.56 $\pm$ 0.06
	MTFIL-Net[34]	91.34 $\pm$ 2.53	92.95 $\pm$ 1.99	90.52 $\pm$ 9.61	98.58 $\pm$ 1.04	5.21 $\pm$ 0.64	0.64 $\pm$ 0.06
	MTI-Net[35]	90.43 $\pm$ 4.35	90.43 $\pm$ 7.54	90.43 $\pm$ 11.63	97.82 $\pm$ 0.74	5.42 $\pm$ 0.46	0.62 $\pm$ 0.07
	MTDL	<b>93.63 <math>\pm</math> 2.21</b>	<b>94.13 <math>\pm</math> 2.58</b>	<b>93.23 <math>\pm</math> 4.58</b>	<b>99.16 <math>\pm</math> 1.14</b>	<b>4.78 <math>\pm</math> 0.24</b>	<b>0.72 <math>\pm</math> 0.03</b>

external validation sets and obtain sensitivity maps for both tasks separately. We use max pooling and trilinear interpolation as the down-sampling and up-sampling methods for sensitivity maps, respectively. We then project the obtained sensitivity map onto the MNI152 standard template to observe the connection between the ROI and the hippocampus.

As shown in Figure 6, we visualize the sensitivity maps of the subjects through the software Mango (<http://ric.uthscsa.edu/mango/>), and show the hippocampus location on the same slice. We find that although the ROIs for these two tasks are not identical, they are generally highly correlated. This allows the model to be optimized using the correlation between MMSE scores and AD. This means that it can exchange ROIs for different tasks to enhance the robustness of features.

## 5.2 The components of multi-task interaction layer

For AD detection and MMSE score prediction, we propose a multi-task interaction layer including feature decoupling and feature interaction. The feature decoupling module filters the features from the task backbone and implements feature shunting according to generalization. To explore the performance of the feature decoupling module, we remove the feature decoupling modules in MTDL and name it  $\text{MTDL}_{\text{NonD}}$ .  $\mathcal{L}_M$  is used to achieve more efficient feature decoupling. Hence,  $\mathcal{L}_M$  is also removed from  $\text{MTDL}_{\text{NonD}}$ . As shown in Table 5, the experimental results verify the effectiveness of the feature decoupling module. The feature decoupling module realizes the selection of generalizable features and feature shunting, which effectively improves the performance of the model.

Furthermore, our proposed feature interaction module contains two paths. Both linear transformation and convolution provide useful information. To further explore the role of these two parts in feature interaction, we remove linear transformation and convolution in the feature interaction module and name them  $\text{MTDL}_{\text{NonL}}$  and  $\text{MTDL}_{\text{NonConv}}$ , respectively. As shown in Table 5, the experimental results show that both linear transformation and convolution provide beneficial information for feature interactions.

A feature interaction module composed of two paths better captures the shared features for AD detection and MMSE score prediction.

## 5.3 Limitation and future work

Although our proposed method achieves satisfactory results, there are still some issues that need further research. Firstly, our method is validated on multiple sites, but these datasets still contain a small number of subjects. Therefore, more data should be used to validate our proposed MTDL. Secondly, we exploit the correlation of MMSE scores with AD detection for multi-task learning. However, MMSE scores are only one of the indicators that have a correlation with AD. The relationship between other indicators such as clinical dementia rating (CDR) and detection of AD is also worth exploring. In the end, we only use MRI images as network input. It is worth mentioning that multimodal data, which can provide richer patient information, are being used more and more widely. Therefore, the relationship between AD detection and MMSE score prediction can be better explored using multimodal data.

## 6 Conclusion

In summary, we propose a multi-task learning method called MTDL for AD detection and MMSE score prediction. We design a multi-task feature interaction layer to exploit feature correlations between tasks. The feature consistency loss is used to enhance the generalization of the features selected by the feature decoupling module. The distribution loss is used to introduce the distribution information of the MMSE scores to further improve the model performance. We evaluate the proposed method on multi-site datasets. Experimental results show that our method achieves encouraging performance, outperforming other state-of-the-art methods. This method can be used as a reliable AD detection and MMSE score prediction method. It can provide a technical basis for disease diagnosis with correlation, and can also provide reference for other multi-task learning methods.

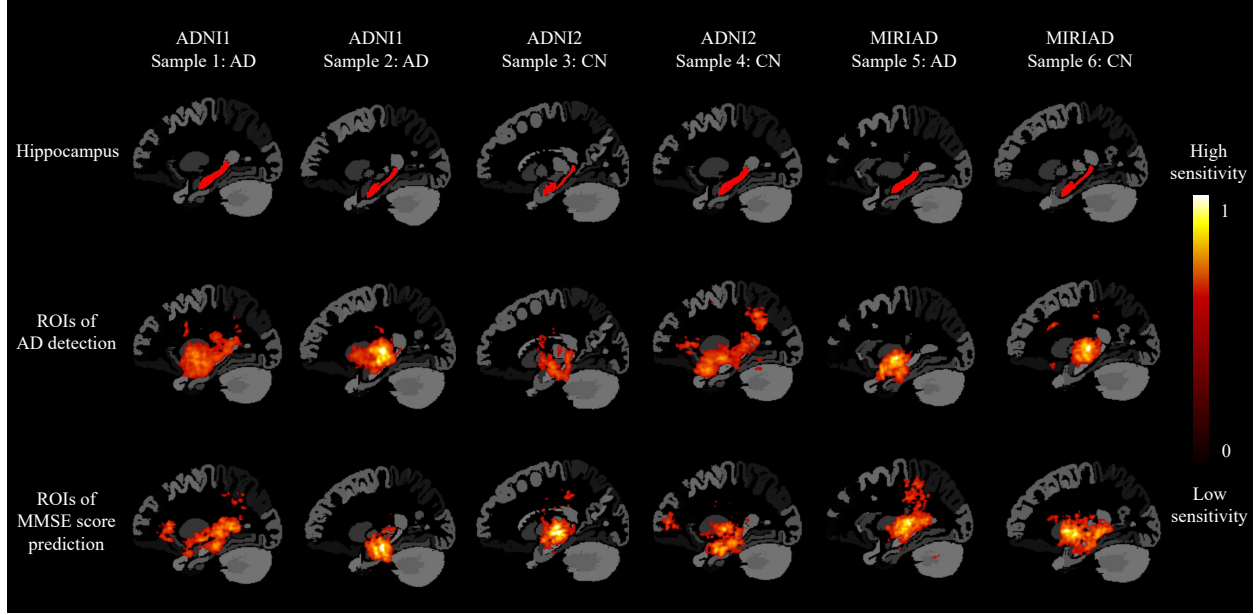


Figure 6: Sagittal view of hippocampus and sensitivity map and of multiple subjects. One column corresponds to one subject. The three rows from top to bottom represent the hippocampus, the ROIs of the AD detection and the ROIs of the MMSE score prediction.

Table 5: Comparison of AD detection and MMSE score prediction performance of  $MTDL_{NonD}$ ,  $MTDL_{NonL}$ ,  $MTDL_{NonConv}$  and  $MTDL$  (mean  $\pm$  std)

Datasets	Methods	AD detection				MMSE score prediction	
		ACC (%)	SEN (%)	SPE (%)	AUC (%)	RMSE	r
ADNI1	$MTDL_{NonD}$	81.84 $\pm$ 5.56	77.35 $\pm$ 12.15	85.66 $\pm$ 12.35	91.42 $\pm$ 3.97	2.55 $\pm$ 0.11	0.70 $\pm$ 0.07
	$MTDL_{NonL}$	83.65 $\pm$ 7.23	79.61 $\pm$ 14.54	87.09 $\pm$ 7.78	91.35 $\pm$ 6.48	2.83 $\pm$ 0.57	0.71 $\pm$ 0.08
	$MTDL_{NonConv}$	82.38 $\pm$ 5.83	79.14 $\pm$ 8.83	85.19 $\pm$ 6.15	92.47 $\pm$ 5.35	3.00 $\pm$ 0.39	0.65 $\pm$ 0.08
	<b>MTDL</b>	<b>87.26 <math>\pm</math> 4.32</b>	<b>84.41 <math>\pm</math> 5.51</b>	<b>89.78 <math>\pm</math> 5.61</b>	<b>94.45 <math>\pm</math> 4.02</b>	<b>2.50 <math>\pm</math> 0.15</b>	<b>0.73 <math>\pm</math> 0.06</b>
ADNI2	$MTDL_{NonD}$	84.34 $\pm$ 3.12	83.59 $\pm$ 8.81	84.83 $\pm$ 7.93	90.90 $\pm$ 1.28	3.06 $\pm$ 0.12	0.75 $\pm$ 0.02
	$MTDL_{NonL}$	84.34 $\pm$ 6.06	<b>84.76 <math>\pm</math> 7.59</b>	84.08 $\pm$ 6.38	<b>93.65 <math>\pm</math> 1.08</b>	3.10 $\pm$ 0.44	0.76 $\pm$ 0.04
	$MTDL_{NonConv}$	82.85 $\pm$ 4.34	81.74 $\pm$ 8.75	83.53 $\pm$ 7.13	93.21 $\pm$ 1.06	3.49 $\pm$ 0.32	0.68 $\pm$ 0.04
	<b>MTDL</b>	<b>86.33 <math>\pm</math> 2.37</b>	78.43 $\pm$ 6.74	<b>91.00 <math>\pm</math> 3.89</b>	93.35 $\pm$ 1.53	<b>2.92 <math>\pm</math> 0.16</b>	<b>0.76 <math>\pm</math> 0.02</b>
MIRIAD	$MTDL_{NonD}$	90.57 $\pm$ 4.72	93.96 $\pm$ 5.89	83.57 $\pm$ 8.06	98.01 $\pm$ 0.01	5.16 $\pm$ 0.37	0.68 $\pm$ 0.04
	$MTDL_{NonL}$	91.88 $\pm$ 4.03	<b>95.43 <math>\pm</math> 4.39</b>	84.78 $\pm$ 10.36	98.37 $\pm$ 0.01	4.95 $\pm$ 0.32	0.71 $\pm$ 0.05
	$MTDL_{NonConv}$	90.66 $\pm$ 3.93	93.47 $\pm$ 5.61	85.02 $\pm$ 11.88	98.21 $\pm$ 0.01	4.98 $\pm$ 0.32	0.70 $\pm$ 0.04
	<b>MTDL</b>	<b>93.63 <math>\pm</math> 2.21</b>	94.13 $\pm$ 2.58	<b>93.23 <math>\pm</math> 4.58</b>	<b>99.16 <math>\pm</math> 1.14</b>	<b>4.78 <math>\pm</math> 0.24</b>	<b>0.72 <math>\pm</math> 0.03</b>

## References

- [1] M. A. DeTure and D. W. Dickson, "The neuropathological diagnosis of alzheimer's disease," *Molecular neurodegeneration*, vol. 14, no. 1, pp. 1–18, 2019.
- [2] D. A. Bennett, J. A. Schneider, Y. Tang, S. E. Arnold, and R. S. Wilson, "The effect of social networks on the relation between alzheimer's disease pathology and level of cognitive function in old people: a longitudinal cohort study," *The Lancet Neurology*, vol. 5, no. 5, pp. 406–412, 2006.
- [3] H. Li, J. Jia, and Z. Yang, "Mini-mental state examination in elderly chinese: a population-based normative study," *Journal of Alzheimer's disease*, vol. 53, no. 2, pp. 487–496, 2016.
- [4] Y. Mu and F. H. Gage, "Adult hippocampal neurogenesis and its role in alzheimer's disease," *Molecular neurodegeneration*, vol. 6, no. 1, pp. 1–9, 2011.
- [5] S. Klöppel *et al.*, "Automatic classification of mr scans in alzheimer's disease," *Brain*, vol. 131, no. 3, pp. 681–689, 2008.
- [6] J. Liu, Y. Pan, F.-X. Wu, and J. Wang, "Enhancing the feature representation of multi-modal mri data by combining multi-view information for mci classification," *Neurocomputing*, vol. 400, pp. 322–332, 2020.
- [7] J. Liu, J. Wang, Z. Tang, B. Hu, F.-X. Wu, and Y. Pan, "Improving alzheimer's disease classification by combining multiple measures," *IEEE/ACM transactions on computational biology and bioinformatics*, vol. 15, no. 5, pp. 1649–1659, 2017.
- [8] M. Liu, D. Zhang, and D. Shen, "Relationship induced multi-template learning for diagnosis of alzheimer's disease and mild cognitive impairment," *IEEE transactions on medical imaging*, vol. 35, no. 6, pp. 1463–1474, 2016.
- [9] J. Liu, M. Li, W. Lan, F.-X. Wu, Y. Pan, and J. Wang, "Classification of alzheimer's disease using whole brain hierarchical network," *IEEE/ACM transactions on computational biology and bioinformatics*, vol. 15, no. 2, pp. 624–632, 2016.
- [10] P. Padilla, M. López, J. M. Górriz, J. Ramirez, D. Salas-Gonzalez, and I. Alvarez, "Nmf-svm based cad tool applied to functional brain images for the diagnosis of alzheimer's disease," *IEEE Transactions on medical imaging*, vol. 31, no. 2, pp. 207–216, 2011.
- [11] J. Islam and Y. Zhang, "Brain mri analysis for alzheimer's disease diagnosis using an ensemble system of deep convolutional neural networks," *Brain informatics*, vol. 5, no. 2, pp. 1–14, 2018.
- [12] J. Wen *et al.*, "Convolutional neural networks for classification of alzheimer's disease: Overview and reproducible evaluation," *Medical image analysis*, vol. 63, p. 101694, 2020.
- [13] K. He, X. Zhang, S. Ren, and J. Sun, "Deep residual learning for image recognition," in *Proceedings of the IEEE conference on computer vision and pattern recognition*, 2016, pp. 770–778.
- [14] K. Simonyan and A. Zisserman, "Very deep convolutional networks for large-scale image recognition," *arXiv preprint arXiv:1409.1556*, 2014.
- [15] M. Liu, J. Zhang, E. Adeli, and D. Shen, "Landmark-based deep multi-instance learning for brain disease diagnosis," *Medical image analysis*, vol. 43, pp. 157–168, 2018.
- [16] J. Zhang, Y. Gao, Y. Gao, B. C. Munsell, and D. Shen, "Detecting anatomical landmarks for fast alzheimer's disease diagnosis," *IEEE transactions on medical imaging*, vol. 35, no. 12, pp. 2524–2533, 2016.
- [17] K. Aderghal, A. Khvostikov, A. Krylov, J. Benois-Pineau, K. Afdel, and G. Catheline, "Classification of alzheimer disease on imaging modalities with deep cnns using cross-modal transfer learning," in *2018 IEEE 31st international symposium on computer-based medical systems (CBMS)*. IEEE, 2018, pp. 345–350.
- [18] C. Lian, M. Liu, J. Zhang, and D. Shen, "Hierarchical fully convolutional network for joint atrophy localization and alzheimer's disease diagnosis using structural mri," *IEEE transactions on pattern analysis and machine intelligence*, vol. 42, no. 4, pp. 880–893, 2018.
- [19] S. Qiu *et al.*, "Development and validation of an interpretable deep learning framework for alzheimer's disease classification," *Brain*, vol. 143, no. 6, pp. 1920–1933, 2020.
- [20] S. Kovacevic, M. S. Rafii, J. B. Brewer *et al.*, "High-throughput, fully-automated volumetry for prediction of mmse and cdr decline in mild cognitive impairment," *Alzheimer disease and associated disorders*, vol. 23, no. 2, p. 139, 2009.
- [21] L. Huang *et al.*, "Longitudinal clinical score prediction in alzheimer's disease with soft-split sparse regression based random forest," *Neurobiology of aging*, vol. 46, pp. 180–191, 2016.
- [22] S. Tabarestani *et al.*, "A distributed multitask multimodal approach for the prediction of alzheimer's disease in a longitudinal study," *NeuroImage*, vol. 206, p. 116317, 2020.
- [23] M. Liu, J. Zhang, C. Lian, and D. Shen, "Weakly supervised deep learning for brain disease prognosis using mri and incomplete clinical scores," *IEEE transactions on cybernetics*, vol. 50, no. 7, pp. 3381–3392, 2019.
- [24] N. T. Duc, S. Ryu, M. N. I. Qureshi, M. Choi, K. H. Lee, and B. Lee, "3d-deep learning based automatic diagnosis of alzheimer's disease with joint mmse prediction using resting-state fmri," *Neuroinformatics*, vol. 18, no. 1, pp. 71–86, 2020.
- [25] X. Zhu, H.-I. Suk, and D. Shen, "A novel matrix-similarity based loss function for joint regression and classification in ad diagnosis," *NeuroImage*, vol. 100, pp. 91–105, 2014.
- [26] M. Liu, J. Zhang, E. Adeli, and D. Shen, "Joint classification and regression via deep multi-task multi-channel learning for alzheimer's disease diagnosis," *IEEE Transactions on Biomedical Engineering*, vol. 66, no. 5, pp. 1195–1206, 2018.
- [27] S. El-Sappagh, T. Abuhmed, S. R. Islam, and K. S. Kwak, "Multimodal multitask deep learning model for alzheimer's disease progression detection based on time series data," *Neurocomputing*, vol. 412, pp. 197–215, 2020.
- [28] J. Hu, L. Shen, and G. Sun, "Squeeze-and-excitation networks," in *Proceedings of the IEEE conference on computer vision and pattern recognition*, 2018, pp. 7132–7141.

- [29] S. Woo, J. Park, J.-Y. Lee, and I. S. Kweon, “Cbam: Convolutional block attention module,” in *Proceedings of the European conference on computer vision (ECCV)*, 2018, pp. 3–19.
- [30] I. Misra, A. Shrivastava, A. Gupta, and M. Hebert, “Cross-stitch networks for multi-task learning,” in *Proceedings of the IEEE conference on computer vision and pattern recognition*, 2016, pp. 3994–4003.
- [31] M. Jenkinson, C. F. Beckmann, T. E. Behrens, M. W. Woolrich, and S. M. Smith, “Fsl,” *Neuroimage*, vol. 62, no. 2, pp. 782–790, 2012.
- [32] D. P. Kingma and J. Ba, “Adam: A method for stochastic optimization,” *arXiv preprint arXiv:1412.6980*, 2014.
- [33] Y. Gao, J. Ma, M. Zhao, W. Liu, and A. L. Yuille, “Nddr-cnn: Layerwise feature fusing in multi-task cnns by neural discriminative dimensionality reduction,” in *Proceedings of the IEEE/CVF Conference on Computer Vision and Pattern Recognition*, 2019, pp. 3205–3214.
- [34] J. Liu, X. Tian, J. Wang, R. Guo, and H. Kuang, “Mtfil-net: automated alzheimer’s disease detection and mmse score prediction based on feature interactive learning,” in *2021 IEEE International Conference on Bioinformatics and Biomedicine (BIBM)*. IEEE, 2021, pp. 1002–1007.
- [35] S. Vandenhende, S. Georgoulis, and L. Van Gool, “Mti-net: Multi-scale task interaction networks for multi-task learning,” in *European Conference on Computer Vision*. Springer, 2020, pp. 527–543.